

Surface plasmons in metallic structures

J M Pitarke^{1,2}, V M Silkin², E V Chulkov^{2,3} and P M Echenique^{2,3}

¹ Materia Kondentsatuaren Fisika Saila, Zientzi Fakultatea, Euskal Herriko Unibertsitatea, 644 Posta kutxatila, E-48080 Bilbo, Basque Country, Spain

² Donostia International Physics Centre (DIPC) and Centro Mixto CSIC-UPV/EHU, Manuel de Lardizabal Pasealekua, E-20018 Donostia, Basque Country, Spain

³ Materialen Fisika Saila, Kimika Fakultatea, Euskal Herriko Unibertsitatea, 1072 Posta kutxatila, E-20080 Donostia, Basque Country, Spain

Received 22 June 2004, accepted for publication 5 August 2004

Published 20 January 2005

Online at stacks.iop.org/JOptA/7/S73

Abstract

Since the concept of a surface collective excitation was first introduced by Ritchie, surface plasmons have played a significant role in a variety of areas of fundamental and applied research, from surface dynamics to surface-plasmon microscopy, surface-plasmon resonance technology, and a wide range of photonic applications. Here we review the basic concepts underlying the existence of surface plasmons in metallic structures, and introduce a new low-energy surface collective excitation that has been recently predicted to exist.

Keywords: electrons, surfaces, collective effects, polaritons, optical absorption, many-body, particle–solid interactions

1. Introduction

The long-range nature of the Coulomb interaction between valence electrons in metals is known to yield collective behaviour, manifesting itself in the form of plasma oscillations. Pines and Bohm [1] were the first to suggest that the discrete energy losses experienced by fast electrons in passing through metals are due to the excitation of these plasma oscillations, the basic unit of energy being termed the plasmon [2]: $\hbar\omega_p = \hbar(4\pi ne^2/m_e)^{1/2}$, where n is the valence electron density and m_e is the free-electron mass⁴.

Gabor [3] investigated the excitation of plasma oscillations in thin foils, but assumed that the electric field is always zero at the surface. As a result, he did not find surface modes in the bounded plasma and reached the erroneous conclusion that the probability for plasma loss should decrease strongly with decreasing foil thickness. Ritchie [4] was the first to find that the effect of the film boundaries is to cause the appearance of a new ‘lowered’ loss at $\hbar\omega_s = \hbar\omega_p/\sqrt{2}$ due to the excitation of surface collective oscillations, the quanta of which Stern and Ferrell called the surface plasmons [5].

Ritchie’s prediction of surface polarization causing low-energy losses in metals was confirmed in a series of

experiments carried out by Powell and Swan [6], who observed inelastic losses experienced by electrons scattered from newly evaporated layers of Al and Mg. Since then, there has been a significant advance in both theoretical and experimental investigations of collective modes in the vacuum–solid interface.

The concept of the surface plasmon has played a key role in the understanding of fundamental properties of solids and in the interpretation of a large variety of experiments. For example, the classical image potential acting between a point classical charge and a metal surface was shown to be originated in the shifted zero-point energy of the surface-plasmon field [7–10], the impact of the surface plasmon on surface energies was addressed [11], the energy loss of charged particles moving outside a metal surface was shown to be due to the excitation of surface plasmons [12, 13], and the centroid of the electron density induced by external potentials acting on a metal surface was demonstrated to be dictated by the wavevector dependence of surface plasmons [14]. Explicit expressions for the surface-plasmon dispersion relied originally on simple models, such as the hydrodynamic [15], specular-reflection [16], and infinite-barrier [17] models. Accurate numerical calculations have also been performed from the knowledge of the eigenfunctions and eigenvalues of the Kohn–Sham Hamiltonian of density-functional theory (DFT) [18], showing nice agreement with the experiments that have been carried out on clean, well-characterized surfaces of

⁴ The valence electron density n is usually characterized by the density parameter $r_s = (3/4\pi n)^{1/3}/a_0$ (a_0 is the Bohr radius, $a_0 = 0.529$ Å). In metals ($2 < r_s < 6$), plasmons have energies in the range 5 eV $< \omega_p < 20$ eV and frequencies that lie, therefore, in the optical regime.

the alkali metals [19, 20]. These experiments also showed evidence for the existence of the so-called multipole surface plasmons that had been predicted by Benett [21].

The long-wavelength⁵ surface-plasmon energy $\hbar\omega_s$ was derived by Ritchie in the nonrelativistic approximation, by assuming that the Coulomb interaction is instantaneous. However, if one is to describe the interaction of either relativistic electrons or light with solid surfaces, it is necessary to take into account the time needed for the propagation of the true retarded interaction. As a result of retardation, surface plasmons couple at wavelengths larger than $\sim 2\pi c/\omega_s$ with the free electromagnetic field and yield what is now called a surface-plasmon polariton [22]. At these large wavelengths, the surface-plasmon polariton exists over the entire frequency range from zero to an asymptotic value determined by the surface-plasmon frequency ω_s . However, the corresponding dispersion curve never crosses the dispersion curve of free-space electromagnetic radiation. Hence, there is always a momentum mismatch between light and surface plasmons of the same frequency, so light incident on an ideal surface cannot excite surface plasmons and, conversely, the surface plasmon cannot decay by emitting a photon.

Teng and Stern [23] were the first to point out that any surface roughness permits the surface to impart some additional momentum to the surface-plasma oscillation, with the result that it can couple to electromagnetic radiation. Alternatively, prism coupling can be used to enhance the momentum of incident light, as demonstrated by Otto [24] and by Kretschmann and Raether [25]. Hence, surface plasmons have been employed in a wide spectrum of studies from electrochemistry, catalysis, wetting, thin organic condensates, and biosensing [26], to scanning tunnelling microscopy [27], the ejection of ions from surfaces [28], surface dynamics [29], surface-plasmon microscopy [30], and surface-plasmon resonance technology [31]. Moreover, recent advances that allow metals to be structured and characterized on the nanometre scale have rekindled the long-standing interest in surface plasmons, one of the most attractive aspects of these collective excitations now being their use to concentrate light in subwavelength structures [32] and to enhance transmission through periodic arrays of subwavelength holes in optically thick metallic films [33, 34], as well as the possible fabrication of nanoscale photonic circuits operating at optical frequencies [35].

Since the typical energy of bulk and surface plasmons is of a few electronvolts, thermal excitation of these collective oscillations is improbable, so the electronic properties near the Fermi level cannot be directly influenced by these excitations. Much more effective than ordinary bulk and surface plasmons in mediating, e.g., superconductivity would be the so-called acoustic plasmons with sound-like long-wavelength dispersion [36], which have spurred over the years a remarkable interest and research activity [37]. Acoustic plasma oscillations were observed in two-dimensionally confined and spatially separated multicomponent structures such as quantum wells and heterojunctions [38, 39], and were then proposed as possible candidates to mediate the attractive

⁵ Throughout this paper, long wavelengths are associated with low wavevectors.

interaction leading to the formation of Cooper pairs in high- T_c superconductors [40, 41].

Recently, it has been shown that metal surfaces where a partially occupied quasi-two-dimensional (2D) surface-state band coexists in the same region of space as the underlying three-dimensional (3D) continuum support a well-defined acoustic surface plasmon [42]. This *new* low-energy collective excitation exhibits linear dispersion at low wavevectors, and might therefore affect electron–hole (e–h) and phonon dynamics near the Fermi level⁶. It has been demonstrated that it is a combination of the nonlocality of the 3D dynamical screening and the spill out of the 3D electron density into the vacuum which allows the formation of 2D electron-density acoustic oscillations at metal surfaces, since these oscillations would otherwise be completely screened by the surrounding 3D substrate [43].

In this paper, we first present an overview of the basic concepts underlying the existence of surface collective excitations in metallic structures, and we then introduce the new concept of acoustic surface plasmons. We begin in section 2 with a brief discussion of the role that surface-plasmon excitation plays in the interaction of fast charged particles with solid surfaces, since it is precisely the investigation of electron energy loss in thin foils which brought Ritchie to the realization that surface collective excitations exist at the lowered frequency ω_s [4]. The detection of surface plasmons and their dispersion is discussed in section 3, in the framework of angle-resolved inelastic electron scattering experiments. Localized surface plasmons and the use of sum rules that provide insight into surface-plasmon energies in metallic structures of arbitrary geometry are introduced in section 4. Section 5 is devoted to the retarded region, where surface plasmons couple with the free electromagnetic field. Acoustic surface plasmons are introduced in section 6.

Unless stated otherwise, atomic units are used throughout, i.e., $e^2 = \hbar = m_e = 1$.

2. Plasma losses by fast charged particles in solids

Let us consider a recoilless fast point particle of charge Z_1 moving in an arbitrary inhomogeneous many-electron system with nonrelativistic velocity \mathbf{v} , for which retardation effects and radiation losses can be neglected⁷. The charge density of the probe particle is simply a delta function of the form

$$\rho^{\text{ext}}(\mathbf{r}, t) = Z_1 \delta(\mathbf{r} - \mathbf{r}_0 - \mathbf{v}t), \quad (1)$$

and the energy that this classical particle loses per unit time due to electronic excitations in the medium can be written as [44]

$$-\frac{dE}{dt} = - \int d\mathbf{r} \rho^{\text{ext}}(\mathbf{r}, t) \frac{\partial V^{\text{ind}}(\mathbf{r}, t)}{\partial t}, \quad (2)$$

where $V^{\text{ind}}(\mathbf{r}, t)$ is the potential induced by the probe particle at position \mathbf{r} and time t .

⁶ The sound velocity of this acoustic mode is, however, close to the Fermi velocity of the 2D surface-state band, which is typically a few orders of magnitude larger than the sound velocity of acoustic phonons in metals but still about two orders of magnitude smaller than the velocity of light.

⁷ This approximation is valid for heavy charged particles, e.g., ions, and also for swift electrons moving with nonrelativistic velocities that are large compared to the velocity of target electrons. In the case of electrons, $Z_1 = -1$.

To first order in the external perturbation, time-dependent perturbation theory yields

$$V^{\text{ind}}(\mathbf{r}, t) = \int d\mathbf{r}' \int_{-\infty}^{+\infty} dt' \int_{-\infty}^{+\infty} \frac{d\omega}{2\pi} e^{-i\omega(t-t')} \times \tilde{W}(\mathbf{r}, \mathbf{r}'; \omega) \rho^{\text{ext}}(\mathbf{r}', t'), \quad (3)$$

where

$$\tilde{W}(\mathbf{r}, \mathbf{r}'; \omega) = W(\mathbf{r}, \mathbf{r}'; \omega) - v(\mathbf{r}, \mathbf{r}'), \quad (4)$$

$v(\mathbf{r}, \mathbf{r}')$ being the bare Coulomb interaction and $W(\mathbf{r}, \mathbf{r}'; \omega)$ being the so-called screened interaction, which is usually expressed in terms of the density-response function of the many-electron system [45].

Equation (3) is a general expression for the energy loss of a classical particle moving in an arbitrary inhomogeneous electron system that is characterized by the screened interaction $W(\mathbf{r}, \mathbf{r}'; \omega)$. Here we consider a solid target consisting of a fixed uniform positive background (jellium) plus a neutralizing cloud of interacting valence electrons, which will be described by either an infinite or a plane-bounded electron gas.

2.1. Infinite electron gas

In the case of an infinite homogeneous electron gas that is translationally invariant in all directions, equations (1)–(3) yield the following expression for the so-called stopping power, i.e., the energy that the probe particle loses per unit path length:

$$-\frac{dE}{dx} = -Z_1^2 \int \frac{d^3\mathbf{k}}{(2\pi)^3} \mathbf{k} \cdot \mathbf{v} \text{Im} \tilde{W}(k, \mathbf{k} \cdot \mathbf{v}), \quad (5)$$

$\tilde{W}(k, \omega)$ being the 3D Fourier transform of $\tilde{W}(\mathbf{r}, \mathbf{r}'; \omega)$, which is typically expressed in the form

$$\tilde{W}(k, \omega) = \frac{4\pi}{k^2} [\epsilon^{-1}(k, \omega) - 1], \quad (6)$$

where $\epsilon^{-1}(k, \omega)$ is the so-called inverse dielectric function of the electron gas.

At high projectile velocities ($v_F \ll v$, v_F being the Fermi velocity), the zero-point motion of the electron gas can be neglected and it can be considered, therefore, as if it were at rest. In this approximation, the dielectric function $\epsilon(k, \omega)$ of a homogeneous electron gas takes the form [46]

$$\epsilon(k, \omega) = 1 - \frac{\omega_p^2}{\omega(\omega + i\eta) - k^4/4}, \quad (7)$$

which at long wavelengths ($k \rightarrow 0$) yields the classical Drude dielectric function

$$\epsilon(\omega) = 1 - \frac{\omega_p^2}{\omega(\omega + i\eta)}, \quad (8)$$

ω_p being the bulk plasma frequency and η a positive infinitesimal.

The dielectric function of equation (7) describes both collective and single-particle excitations. At wavevectors \mathbf{k} smaller than a cut-off wavevector of magnitude $k_c \sim \omega_p/v_F$, the many-electron system can be expected to behave collectively, losses being dominated by the excitation of plasma oscillations [2]. At wavevectors of magnitude larger

than k_c , losses are dominated by the excitation of e-h pairs. Using equation (7) and assuming that $v \gg v_F$, equation (5) yields

$$-\frac{dE}{dx} = Z_1^2 \frac{\omega_p^2}{v^2} \left[\ln \frac{k_c}{\omega_p/v} + \ln \frac{2v}{k_c} \right], \quad (9)$$

or, equivalently,

$$-\frac{dE}{dx} = Z_1^2 \frac{\omega_p^2}{v^2} \ln \frac{2v^2}{\omega_p}. \quad (10)$$

The first term of equation (9), which can also be obtained by using the Drude dielectric function of equation (8), represents the contribution to the stopping power from losses to collective excitations at wavevectors of magnitude smaller than k_c . The second term of equation (9) represents the contribution from losses to single-particle excitations at wavevectors above k_c .

2.2. Plane-bounded electron gas

In the case of a plane-bounded electron gas that is translationally invariant in two directions, which we take to be normal to the z axis, equations (1)–(3) yield the following expression for the energy that the probe particle loses per unit time:

$$-\frac{dE}{dt} = i \frac{Z_1^2}{\pi} \int \frac{d^2\mathbf{q}}{(2\pi)^2} \int_{-\infty}^{+\infty} dt' \int_0^{\infty} d\omega \omega \times e^{-i(\omega - \mathbf{q} \cdot \mathbf{v}_{\parallel})(t-t')} \tilde{W}[z(t), z(t'); q, \omega], \quad (11)$$

where \mathbf{q} is a 2D wavevector in the plane of the surface, \mathbf{v}_{\parallel} represents the component of the velocity that is parallel to the surface, $z(t)$ represents the position of the projectile relative to the surface, and $\tilde{W}(z, z'; q, \omega)$ is the 2D Fourier transform of $\tilde{W}(\mathbf{r}, \mathbf{r}'; \omega)$.

In the simplest possible model of a bounded semi-infinite electron gas, one characterizes the electron gas at $z \geq 0$ by a local dielectric function which jumps discontinuously at the surface from unity outside ($z < 0$) to $\epsilon(\omega)$ inside ($z > 0$). By imposing the ordinary boundary conditions of continuity of the potential and the normal component of the displacement vector at $z = 0$, one finds

$$\tilde{W}(z, z'; \mathbf{q}, \omega) = \frac{2\pi}{q} \begin{cases} -g(\omega) e^{-q(|z|+|z'|)}, & z < 0, \\ [\epsilon^{-1}(\omega) - 1] e^{-q|z-z'|} & + \epsilon^{-1}(\omega) g(\omega) e^{-q(|z|+|z'|)}, & z > 0, \end{cases} \quad (12)$$

where

$$g(\omega) = \frac{\epsilon(\omega) - 1}{\epsilon(\omega) + 1} \quad (13)$$

is the long-wavelength ($q \rightarrow 0$) limit of the so-called surface-response function [47]. In this limit, the dielectric function $\epsilon(\omega)$ takes the Drude form dictated by equation (8).

In the following, we shall explicitly consider particle trajectories that are normal and parallel to the surface.

2.2.1. Normal trajectory. Let us consider a situation in which the probe particle moves along a normal trajectory from the vacuum side of the surface ($z < 0$) and enters the solid at $z = t = 0$. The position of the projectile relative to the surface is then $z(t) = vt$. Assuming that the electron gas at $z \geq 0$ can be described by the Drude dielectric function of equation (8) and introducing equation (12) into (11), one finds the following expression for the energy that the probe particle loses per unit path length:

$$-\frac{dE}{dz} = \frac{Z_1^2}{v^2} \begin{cases} \omega_s^2 f(2\omega_s|z|/v), & z < 0, \\ \omega_p^2 [\ln(k_c v/\omega_p) - h(\omega_p z/v)] & \\ \quad + \omega_s^2 h(\omega_s z/v), & \\ \omega_s^2 f(2\omega_s|z|/v), & z > 0, \end{cases} \quad (14)$$

where

$$h(\alpha) = 2 \cos(\alpha) f(\alpha) - f(2\alpha), \quad (15)$$

with $f(\alpha)$ being given by the following expression:

$$f(\alpha) = \int_0^\infty \frac{x e^{-\alpha x}}{1+x^2} dx. \quad (16)$$

The Drude dielectric function of equation (8), which assumes that infinitely long-lived plasmons at a single frequency, ω_p , are the only possible bulk excitations, is only sustainable at wavevectors below a cut-off k_c . Hence, this cut-off has been introduced into the bulk (logarithmic) term of equation (14), which yields a contribution to the energy loss that coincides with the plasmon contribution of equation (9). Contributions to the energy loss that are due to the excitation of e-h pairs are not included in equation (14).

In the absence of the boundary at $z = 0$, the position-dependent $f(\alpha)$ and $h(\alpha)$ terms entering equation (14) would not be present, and the energy loss would be that of charged particles moving in an infinite plasma. When the probe particle is moving outside the solid, the effect of the boundary is to cause energy loss at the lowered plasma frequency ω_s . When the probe particle is moving inside the solid, the effect of the boundary is to cause both a decrease in loss at the bulk plasma frequency ω_p and an additional loss at the lowered plasma frequency ω_s , as predicted by Ritchie [4].

Now we consider the real situation in which a fast charged particle passes through a *finite* foil of thickness a (see figure 1). Assuming that the foil is thick enough for the effect of each boundary to be the same as in the case of a semi-infinite medium, and integrating along the whole trajectory from minus to plus infinity, one finds the total energy that the probe particle loses to collective excitations:

$$-\Delta E = \frac{Z_1^2}{v^2} \left[a \omega_p^2 \ln \frac{k_c v}{\omega_p} - \frac{\pi}{2} \omega_p + \pi \omega_s \right]. \quad (17)$$

This is the result first derived by Ritchie in a different way [4], which brought him to the realization that surface collective excitations exist at the lowered frequency ω_s . The first term of equation (17), which is proportional to the thickness of the film, represents the bulk contribution, which would also be present in the absence of the boundaries.

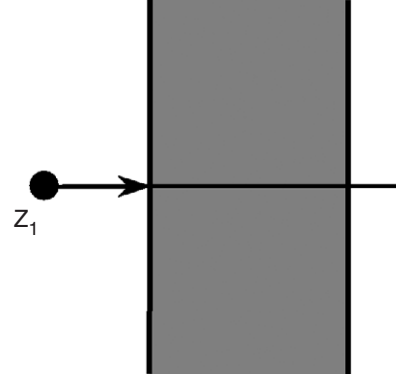


Figure 1. A particle of charge Z_1 passing through a finite foil of thickness a .

The second and third terms, which are both due to the presence of the boundaries and become relatively more important as the foil thickness decreases, represent the decrease in the energy loss at the plasma frequency ω_p and the energy loss at the lowered frequency ω_s , respectively. Equation (17) also shows that the net boundary effect is an increase in the total energy loss above the value which would exist in its absence, as noted by Ritchie [4].

Ritchie also considered the coupling that exists between the two surfaces for finite values of the film thickness a . He found the following dispersion relation between the frequency of surface-plasma oscillations and the wavenumber q :

$$\omega = \omega_s [1 \pm e^{-aq}]^{1/2}, \quad (18)$$

the exponential factor being a consequence of the interaction between the two surfaces. This equation has two limiting cases, as discussed by Ferrell [48]. At short wavelengths ($qa \gg 1$), the surface waves become decoupled and each surface sustains independent oscillations at the reduced frequency ω_s characteristic of a semi-infinite electron gas with a single plane boundary. At long wavelengths ($qa \ll 1$), there are ‘normal’ oscillations at ω_p and ‘tangential’ 2D oscillations at

$$\omega_{2D} = (2\pi naq)^{1/2}, \quad (19)$$

which were later discussed by Stern [49] and observed in artificially structured semiconductors [50] and more recently in a metallic surface-state band on a silicon surface [51].

2.2.2. Parallel trajectory. Now we restrict our attention to the case of charged particles moving with constant velocity at a fixed distance z from the surface (see figure 2). Equation (11) then yields

$$-\frac{dE}{dx} = -\frac{2}{v} Z_1^2 \int \frac{d^2 \mathbf{q}}{(2\pi)^2} \int_0^\infty d\omega \omega \times \text{Im} \tilde{W}(z, z; \mathbf{q}, \omega) \delta(\omega - \mathbf{q} \cdot \mathbf{v}). \quad (20)$$

Assuming that the electron gas at $z \geq 0$ can be described by the Drude dielectric function of equation (8) and introducing

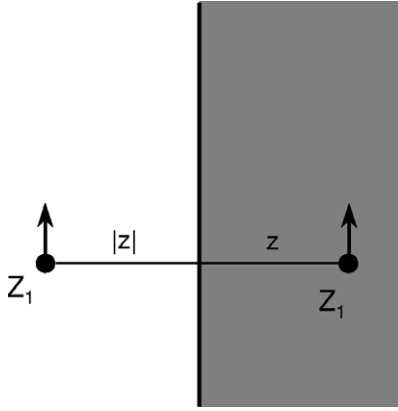


Figure 2. A particle of charge Z_1 moving at a fixed distance z from the surface of a plane-bounded electron gas.

equation (12) into (20), one finds

$$-\frac{dE}{dx} = \frac{Z_1^2}{v^2} \begin{cases} \omega_s^2 K_0(2\omega_s|z|/v), & z < 0, \\ \omega_p^2 [\ln(k_c v/\omega_p) - K_0(2\omega_p z/v)] & \\ \quad + \omega_s^2 K_0(2\omega_s z/v), & \\ z > 0, \end{cases} \quad (21)$$

where $K_0(\alpha)$ is the zero-order modified Bessel function [52].

For particle trajectories outside the solid ($z < 0$), equation (21) reproduces the classical expression of Echenique and Pendry [12]. For particle trajectories inside the solid ($z > 0$), equation (21) reproduces the result first obtained by Nuñez *et al* [53]. As in the case of a normal trajectory, when the particle moves inside the solid the effect of the boundary is to cause a decrease in loss at the bulk plasma frequency ω_p and an additional loss at the lowered plasma frequency ω_s .

3. Inelastic electron scattering

The most commonly used experimental arrangement for detecting surface plasmons by the fields of moving charged particles is based on angle-resolved inelastic electron scattering [54, 55]. Figure 3 shows a schematic drawing of the scattering geometry. A monochromatic beam of electrons, incident on a flat surface at an angle θ_i , is back scattered and detected by an angle-resolved energy analyser positioned at an angle θ_f . Inelastic events can occur, either before or after the elastic event, on exciting a surface mode of frequency $\omega(q)$. The energy and lifetime of this mode are determined by the corresponding energy-loss peak in the spectra, and the momentum q parallel to the surface is obtained from the measured angles θ_i and θ_f .

The inelastic scattering cross section corresponding to a process in which an electronic excitation of energy ω and parallel momentum q is created at the surface of a semi-infinite electron gas is dictated by the imaginary part of the surface-response function $g(q, \omega)$ [47], which in the long-wavelength limit is given by equation (13). In a free-electron gas (jellium), the dielectric function $\epsilon(\omega)$ entering equation (13) is the Drude dielectric function of equation (8). Hence, in a gas of free

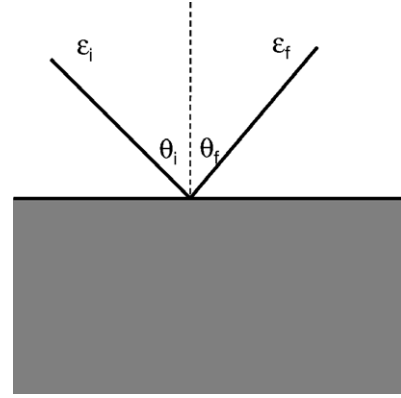


Figure 3. A schematic drawing of the scattering geometry in angle-resolved inelastic electron scattering experiments. On exciting a surface mode of frequency $\omega(q)$, the energy of detected electrons becomes $\epsilon_f = \epsilon_i - \omega(q)$. The momentum q is determined from $q = \sqrt{2} [\sqrt{\epsilon_i} \sin \theta_i - \sqrt{\epsilon_f} \sin \theta_f]$.

electrons $\text{Im } g(q, \omega)$ becomes a delta function peaked at the surface-plasmon energy ω_s .

The classical picture leading to equations (8) and (13), which is correct only in the long-wavelength limit, ignores both the nonlocality of the electronic response of the system and the microscopic spatial distribution of the electron density near the surface. Feibelman showed that up to first order in an expansion in powers of q , the surface-response function of a jellium surface can be written as [14]

$$g(q, \omega) = \frac{\epsilon(\omega) - 1}{\epsilon(\omega) + 1} \left[1 + 2qd_{\perp}(\omega) \frac{\epsilon(\omega)}{\epsilon(\omega) + 1} \right] + O(q^2), \quad (22)$$

where $d_{\perp}(\omega)$ represents the centroid of the induced electron density. Self-consistent density-functional calculations of $g(q, \omega)$ and $d_{\perp}(\omega)$ have demonstrated that in the case of jellium surfaces in the range of typical bulk densities the surface-plasmon energy $\omega(q)$ (where $\text{Im } g(q, \omega)$ is maximum) is at nonvanishing but small q wavevectors lower than ω_s , in agreement with experiment [19, 20]. This is illustrated in figure 4, where the surface-plasmon energy dispersion is drawn schematically, showing that the initial slope is negative. For an interpretation of negative dispersion and comparison to experiment, see [47].

At jellium surfaces, the actual surface-response function reduces in the long-wavelength limit to equation (13) with the Drude $\epsilon(\omega)$ of equation (8), and surface plasmons are therefore expected to be infinitely long-lived excitations. However, energy-loss measurements at simple metal surfaces indicate that surface plasmons exhibit a finite width even at $q = 0$ [56]. Since surface plasmons are dictated in this $q = 0$ limit by bulk properties through the dielectric function $\epsilon(\omega)$, the experimental surface-plasmon widths $\Delta\omega_s$ at $q = 0$ should be approximately described by using in equation (13) the measured bulk dielectric function $\epsilon(\omega)$ instead of its Drude counterpart. Table 1 exhibits the relative widths $\Delta\omega_s/\omega_s$ of surface plasmons derived in this way [47], together with surface-loss measurements at $q = 0$ [56]. Although in the case of Ag, Li, Hg, and Mg the surface-plasmon width is well described by introducing the measured bulk dielectric function into equation (13), the surface-plasmon widths of K and Al are

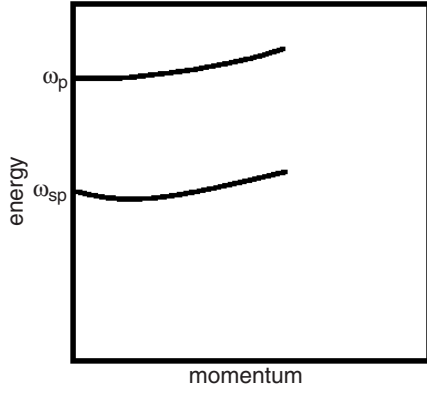


Figure 4. A schematic drawing of the bulk and surface-plasmon energy dispersions in typical metal surfaces. While in the case of bulk plasmons the initial slope is usually (but not always) positive, the surface-plasmon energy dispersion is negative for typical metal surfaces.

Table 1. Relative widths $\Delta\omega_s/\omega_s$ of surface plasmons, as derived from the imaginary part of the surface-response function of equation (13) with measured values of the bulk dielectric function $\epsilon(\omega)$ (theory) [47] and from the surface-loss measurements at $q = 0$ (experiment) [56].

	Ag	K	Al	Mg	Hg	Li
Theory	0.027	0.035	0.035	0.16	0.18	0.33
Experiment	0.027	0.1	0.24	0.16	0.16	0.35

considerably larger than predicted in this simple way. This shows that an understanding of surface-plasmon broadening mechanisms requires a careful analysis of the actual band structure of the solid. Approximate treatments of the impact of the band structure on the surface-plasmon energy dispersion have been developed by several authors [57–61], but a first-principles description of surface energy-loss measurements has not been carried out yet.

4. Sum rules

Sum rules have played a key role in providing insight in the investigation of a variety of physical situations. A useful sum rule for the surface modes in complementary media with arbitrary geometry was introduced by Apell *et al* [62], which in the special case of a metal/vacuum interface implies that [63]

$$\omega_{s_1}^2 + \omega_{s_2}^2 = \omega_p^2, \quad (23)$$

where ω_{s_1} is the surface-mode frequency of our system, and ω_{s_2} represents the surface mode of a second complementary system in which the regions of plasma and vacuum are interchanged (see figure 5).

For example, a half-space filled with a metal of bulk plasma frequency ω_p and interfaced with vacuum maps into itself (see figure 5), and therefore equation (23) yields

$$\omega_{s_1} = \omega_{s_2} = \omega_p/\sqrt{2}, \quad (24)$$

which is the frequency of plasma oscillations at a metal/vacuum planar interface.

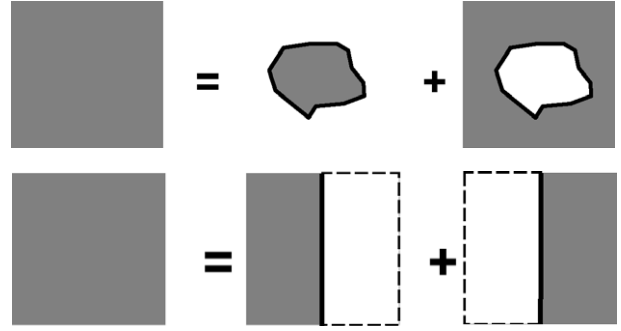


Figure 5. Complementary systems in which the regions of plasma and vacuum are interchanged. The top panel represents the general situation. The bottom panel represents a half-space filled with metal and interfaced with vacuum. The surface-mode frequencies ω_{s_1} and ω_{s_2} of these systems fulfil the sum rule of equation (23).

Other examples are a metal sphere in vacuum, which sustains *localized* Mie plasmons at frequencies

$$\omega_l = \omega_p \sqrt{\frac{l}{2l+1}}, \quad (25)$$

with $l = 1, 2, \dots$, and a spherical void in a metal, which shows Mie plasmons at frequencies

$$\omega_l = \omega_p \sqrt{\frac{l+1}{2l+1}}. \quad (26)$$

The squared surface-mode frequencies of the sphere (equation (25)) and the void (equation (26)) add up to ω_p^2 for all l , as required by equation (23).

Now we consider a situation in which there are two interfaces, as occurs in the case of a thin film and approximately occurs in the case of multishell fullerenes [64] and carbon nanotubes [65]. Apell *et al* [62] have proved a second sum rule, which relates the surface modes corresponding to the in-phase and out-of-phase linear combinations of the screening charge densities at the interfaces. In the case of metal/vacuum interfaces this sum rule takes the form of equation (23), but now ω_{s_1} and ω_{s_2} being in-phase and out-of-phase modes of the same system.

For a Drude metal film with equal and abrupt planar surfaces, the actual values of ω_{s_1} and ω_{s_2} are those given by equation (18). For a spherical fullerene molecule described by assigning a Drude dielectric function to every point between the inner and outer surfaces of radii r_1 and r_2 (see figure 6), one finds the following frequencies for the in-phase and out-of-phase surface modes [66]:

$$\omega_s^2 = \frac{\omega_p^2}{2} \left[1 \pm \frac{1}{2l+1} \sqrt{1 + 4l(l+1)(r_1/r_2)^{2l+1}} \right], \quad (27)$$

which fulfil the sum rule dictated by equation (23).

5. Surface-plasmon polaritons

Planar surface plasmons are known to be traced to the peaks of the imaginary part of the surface-response function $g(q, \omega)$ [47], which in the long-wavelength limit is

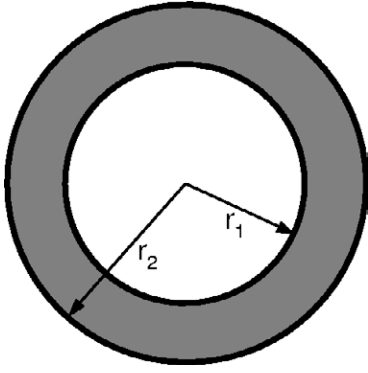


Figure 6. A fullerene molecule of inner and outer radii r_1 and r_2 . A Drude dielectric function is assigned to every point between the inner and outer surfaces.

given by equation (13). This equation yields the *classical* nondispersive surface-plasmon frequency ω_s given by

$$\epsilon(\omega_s) + 1 = 0, \quad (28)$$

which in the case of a semi-infinite Drude metal (see equation (8)) is $\omega_s = \omega_p/\sqrt{2}$.

The long-wavelength surface-plasmon condition of equation (28) has been derived in the nonrelativistic approximation, by neglecting retardation of the Coulomb interaction. Hence, equation (28) yields a good representation of surface-plasma oscillations only at wavelengths that are large compared to the Fermi wavelength ($q \ll k_F \sim 1 \text{ \AA}^{-1}$, k_F being the Fermi momentum) but small compared to the wavelength of light at optical frequencies ($q \gg \omega_s/c \sim 0.005 \text{ \AA}^{-1}$). In a typical inelastic electron scattering experiment, however, the finite angular acceptance of the energy-loss spectrometer guarantees that the momentum transfer q is larger than ω_s/c , so the retarded region of the surface-plasmon dispersion is not observed [67].

Considering the full set of Maxwell equations and still assuming that the wavelength is long enough for a classical description of the metal/vacuum interface to be justified ($q \ll k_F$), one finds that due to retardation the surface-plasmon condition of equation (28) must be replaced by [67]

$$\frac{\epsilon(\omega_s)}{\kappa(\omega_s)} + \frac{1}{\kappa'(\omega_s)} = 0, \quad (29)$$

where

$$\kappa(\omega) = \sqrt{q^2 - \epsilon(\omega) \frac{\omega^2}{c^2}} \quad (30)$$

and

$$\kappa'(\omega) = \sqrt{q^2 - \frac{\omega^2}{c^2}}. \quad (31)$$

In the case of a semi-infinite Drude metal, equations (29)–(31) yield the surface-plasmon dispersion

$$\omega^2(q) = \omega_p^2/2 + c^2 q^2 - \sqrt{\omega_p^4/4 + c^4 q^4}, \quad (32)$$

or, equivalently,

$$q(\omega) = \frac{\omega}{c} \sqrt{\frac{\omega^2 - \omega_p^2}{2\omega^2 - \omega_p^2}}, \quad (33)$$

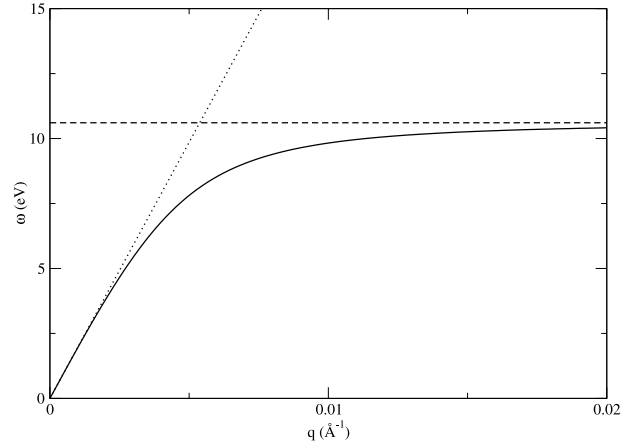


Figure 7. The solid curve represents the dispersion of surface-plasmon polaritons on a semi-infinite Drude metal with $\omega_p = 15 \text{ eV}$, as obtained from equation (32). In the retarded region ($q < \omega_p/c$), the surface-plasmon polariton dispersion curve approaches the light line $\omega = cq$ (dotted line). At short wavelengths ($q \gg \omega/c$), the dispersion curve approaches asymptotically the nonretarded surface-plasmon frequency $\omega_s = \omega_p/\sqrt{2}$ (dashed line).

which we have represented in figure 7 by a solid curve, together with the nonretarded surface-plasmon frequency ω_s (dashed line) and the light line $\omega = cq$ (dotted line). In the retarded region, where $q < \omega_s/c$, surface plasmons couple with the free electromagnetic field, thereby becoming what is called a surface-plasmon polariton. In the nonretarded limit ($q \gg \omega_s/c$), one finds the nondispersive surface-plasmon frequency ω_s .

Significant deviations from the classical surface-plasmon dispersion of equation (32) (like the negative dispersion drawn in figure 4), which are typically observed in electron scattering experiments, are only present at wavevectors larger than those considered in figure 7. At \mathbf{q} wavevectors in the range $\omega_s/c \ll q \ll k_F$, the surface plasmon does not disperse.

6. Acoustic surface plasmons

A variety of metal surfaces, such as Be(0001) and the (111) surfaces of the noble metals Cu, Ag, and Au, are known to support a partially occupied band of Shockley surface states with energies near the Fermi level (see figure 8) [68]. Since these states are strongly localized near the surface and disperse with momentum parallel to the surface, they can be considered to form a quasi-2D surface-state band with a 2D Fermi energy equal to the surface-state binding energy at the $\bar{\Gamma}$ point (see table 2).

In the absence of the 3D substrate, Shockley surface states would support a 2D collective oscillation, the energy of this plasmon being given by equation (19) with na replaced by the 2D density of occupied surface states: $n^{2D} = \epsilon_F^{2D}/\pi$. Equation (19) shows that at very long wavelengths, plasmons in a 2D electron gas have low energies; however, they do not affect e-h and phonon dynamics near the Fermi level, due to their square-root dependence on the wavevector. Much more effective than ordinary 2D plasmons in mediating, e.g., superconductivity would be the so-called acoustic plasmons with sound-like long-wavelength dispersion.

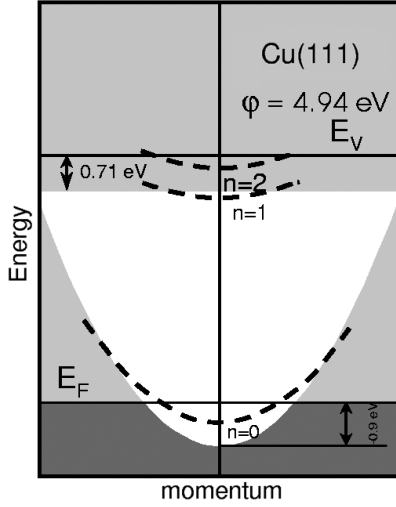


Figure 8. A schematic representation of the surface band structure on Cu(111) near the $\bar{\Gamma}$ point. The shaded region represents the projection of the bulk bands.

Table 2. Binding energies (ϵ_F^{2D}) of surface states at the $\bar{\Gamma}$ point of Be(0001) and the (111) surfaces of the noble metals Cu, Ag, and Au. v_F^{2D} and m^{2D} represent the corresponding 2D Fermi velocity and effective mass, respectively. v_F^{2D} is expressed in units of the Bohr velocity $v_0 = e^2/\hbar$.

	ϵ_F^{2D} (eV)	v_F^{2D}/v_0	m^{2D}
Be(0001)	2.8	0.41	1.18
Cu(111)	0.44	0.28	0.42
Ag(111)	0.065	0.11	0.44
Au(111)	0.48	0.35	0.28

Here we show that in the presence of the 3D substrate the dynamical screening at the surface provides a mechanism for the existence of a *new* acoustic collective mode, whose energy exhibits a linear dependence on the 2D wavenumber.

6.1. A simple model

First of all, we consider a simplified model in which surface-state electrons comprise a 2D electron gas at $z = z_d$ (see figure 9), while all other states of the semi-infinite metal comprise a 3D substrate at $z \leq 0$ represented by the Drude dielectric function of equation (8). Within this model, one finds that both e-h and collective excitations occurring within the 2D gas can be described with the use of an effective 2D dielectric function, which in the random-phase approximation (RPA) takes the form [43]

$$\epsilon_{\text{eff}}^{2D}(q, \omega) = 1 - \left[\frac{2\pi}{q} + \tilde{W}(z_d, z_d; q, \omega) \right] \chi_{2D}^0(q, \omega), \quad (34)$$

$\tilde{W}(z, z'; q, \omega)$ being the screened interaction of equation (12), and $\chi_{2D}^0(q, \omega)$ being the noninteracting density-response function of a 2D electron gas [49].

In the absence of the 3D substrate, $\tilde{W}(z, z'; q, \omega)$ is simply zero and $\epsilon_{\text{eff}}^{2D}(q, \omega)$ coincides, therefore, with the RPA dielectric function of a 2D electron gas, which in the long-wavelength ($q \rightarrow 0$) limit has one single zero corresponding to collective excitations at $\omega = \omega_{2D}$.

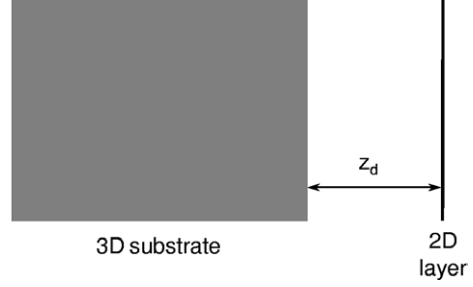


Figure 9. Surface-state electrons comprise a 2D sheet of interacting free electrons at $z = z_d$. All other states of the semi-infinite metal comprise a plane-bounded 3D electron gas at $z \leq 0$. The metal surface is located at $z = 0$.

In the presence of a 3D substrate that is *spatially separated* from the 2D sheet ($z_d > 0$), the long-wavelength limit of $\epsilon_{\text{eff}}^{2D}(q, \omega)$ has two zeros. One zero corresponds to a high-frequency oscillation of energy $\omega^2 = \omega_s^2 + \omega_{2D}^2$ in which 2D and 3D electrons oscillate in phase with one another. The other zero corresponds to a low-frequency *acoustic* oscillation in which both 2D and 3D electrons oscillate out of phase. The energy of this low-frequency mode is found to be of the form [43]

$$\omega = \alpha v_F^{2D} q, \quad (35)$$

with $\alpha > 1$. For small values of the z_d coordinate ($z_d \ll 1$), $\alpha \rightarrow 1$ and the sound velocity approaches, therefore, the Fermi velocity of the 2D sheet. For $z_d \gg 1$, the noninteracting 2D density-response function takes the Drude form $(1/2\pi)(v_F^{2D} q/\omega)^2$, and one finds

$$\alpha = \sqrt{2z_d}, \quad (36)$$

which is the result first obtained by Chaplik in his study of charge-carrier crystallization in low-density inversion layers [69].

If the 2D sheet is located inside the 3D substrate ($z \leq 0$), however, the long-wavelength limit of the effective 2D dielectric function of equation (34) has no zero at low energies ($\omega < \omega_s$), due to a complete screening at these energies of electron–electron interactions within the 2D sheet. This result has suggested over the years that acoustic plasmons should only exist in the case of *spatially separated* plasmas, as pointed out by Das Sarma and Madhukar [38].

Nevertheless, Silkin *et al* [42] have shown that metal surfaces where a partially occupied quasi-2D surface-state band *coexists* in the same region of space as the underlying 3D continuum do support a well-defined acoustic surface plasmon, which could not be explained within the *local* model described above. Furthermore, it has been demonstrated that it is a combination of the nonlocality of the 3D dynamical screening and the spilling out of the 3D electron density into the vacuum which allows the formation of 2D electron-density acoustic oscillations at metal surfaces, since these oscillations would otherwise be completely screened by the surrounding 3D substrate [43].

6.2. Full calculation

In order to achieve a full description of the dynamical response of real metal surfaces, we first consider a one-dimensional

single-particle potential that describes the main features of the surface band structure [70, 71]. We then calculate the eigenfunctions and eigenvalues of the corresponding Hamiltonian, and we evaluate the dynamical density-response function $\chi^0(z, z'; q, \omega)$. Finally, we solve an integral equation to obtain the RPA interacting density-response function $\chi(z, z'; q, \omega)$. From the knowledge of this function, which describes bulk and surface states on the same footing, one can obtain within linear-response theory the electron density induced by an external perturbation $\phi^{\text{ext}}(z; q, \omega)$:

$$\delta n(z; q, \omega) = \int dz' \chi(z, z'; q, \omega) \phi^{\text{ext}}(z'; q, \omega), \quad (37)$$

and the collective excitations created by an external potential of the form

$$\phi^{\text{ext}}(z; q, \omega) = -(2\pi/q)e^{qz} \quad (38)$$

can then be traced to the peaks of the imaginary part of the surface-response function [47]

$$\text{Im}[g(q, \omega)] = \int dz e^{qz} \text{Im}[\delta n(z; q, \omega)]. \quad (39)$$

In the bottom panel of figure 10 we show the result that we have obtained for the unperturbed electron density of the (0001) surface of Be. We see bulk states, whose total density extends to the interior of the solid at $z < 0$, and surface states which are largely localized near the surface. For comparison, we have also carried out a self-consistent jellium density-functional calculation of the electron density (top panel of figure 10), by simply replacing the ions of the solid by a fixed uniform positive background. Surface states are absent in this model.

RPA calculations of the imaginary part of the electron density $\delta n(z; q, \omega)$ induced in a Be(0001) surface by the external potential of equation (38) were reported in [42] for $q = 0.05 a_0^{-1}$ (a_0 is the Bohr radius, $a_0 = 0.529 \text{ \AA}$) and a wide range of frequencies. It was demonstrated that this quantity exhibits two distinct special features, where $\text{Im}[\delta n(q, \omega)]$ is maximum near the surface. The first feature occurs near the surface-plasmon frequency of valence ($2s^2$) electrons in Be ($\hbar\omega_s = 12.8 \text{ eV}$). The second feature occurs at $\omega = 0.6 \text{ eV}$, corresponding to a *new* low-energy acoustic collective oscillation, which had been overlooked over the years.

In figure 11 we show by black lines our full RPA calculation of $\text{Im}[\delta n(z; q, \omega)]$ at $q = 0.05 a_0^{-1}$ and the frequencies $\omega = 12.8 \text{ eV}$ (top panel) and $\omega = 0.6 \text{ eV}$ (bottom panel) at which surface collective oscillations occur. At the conventional surface-plasmon frequency $\omega = 12.8 \text{ eV}$ we have also carried out a jellium density-functional calculation for a semi-infinite free-electron gas, which we have represented by a grey line in the top panel of figure 11. A comparison of our band structure and jellium calculations (black and grey lines) indicates that the conventional surface plasmon is reasonably well described within a jellium model of the surface, although Friedel oscillations in the interior of the solid are considerably more damped in the presence of the actual band structure of the solid.

At the acoustic surface-plasmon energy, which for $q = 0.05 a_0^{-1}$ is $\omega = 0.6 \text{ eV}$, a quasi-2D surface-state band in the presence of a 3D substrate yields the *new* feature displayed

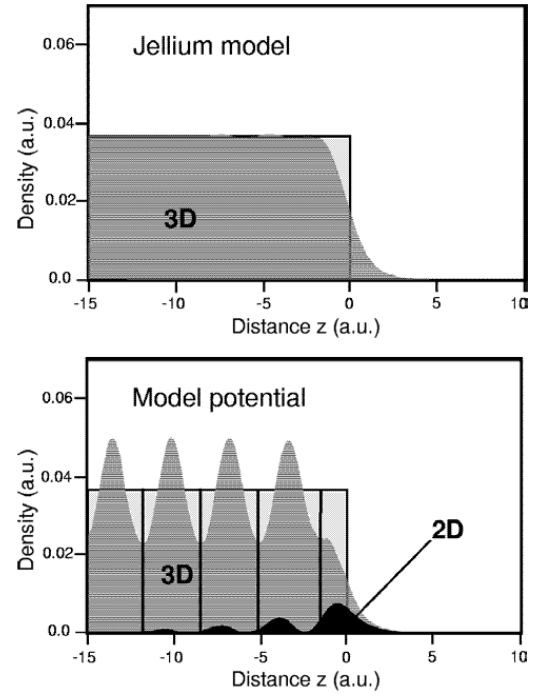


Figure 10. The unperturbed electron density of the (0001) surface of Be (dark grey shaded areas), as obtained from a self-consistent jellium density-functional calculation (top panel) and from the use of a one-dimensional potential that describes the main features of the surface band structure (bottom panel). The light grey shaded areas represent the neutralizing uniform positive background. The vertical lines and black area in the bottom panel, which are absent in the top panel, represent the atomic positions of the solid and the unperturbed density of occupied surface states, respectively. The crystal edge ($z = 0$) is chosen to be located half a lattice spacing beyond the last atomic layer, and $z < 0$ corresponds to the interior of the solid.

in the bottom panel of figure 11. Also shown in this figure (shaded area) is the probability density of the partially occupied Shockley surface state, clearly indicating that the low-energy collective excitation at $\omega = 0.6 \text{ eV}$ originates from this 2D surface-state band. Such a 2D electron gas *alone* would only support a plasmon that for $q = 0.05 a_0^{-1}$ has energy $\omega_{2D} = 2.7 \text{ eV}$, well above the low-energy excitation that is visible in the bottom panel of figure 11, and it is only the combination of the strongly localized 2D surface-state band with 3D bulk states which allows the formation of this new mode.

Figure 12 shows the imaginary part of the surface-response function $g(q, \omega)$ of Be(0001), as obtained from equation (39) for increasing values of q . This figure clearly shows that the excitation spectra is dominated at low energies by a well-defined *acoustic* peak with *linear* dispersion, the sound velocity being at long wavelengths very close to the 2D Fermi velocity v_F^{2D} (see table 2).

In the bottom panel of figure 13 we show the energy of the acoustic surface plasmon in Be(0001) versus the wavenumber q (thick solid line), as derived from the maxima of our calculated surface-loss function $\text{Im}[g(q, \omega)]$ of figure 12. The plasmon energy of electrons in an isolated 2D electron gas would exhibit at long wavelengths a square-root dispersion with the wavenumber q (see equation (19)). However, the combination of a 2D surface-state band with the underlying

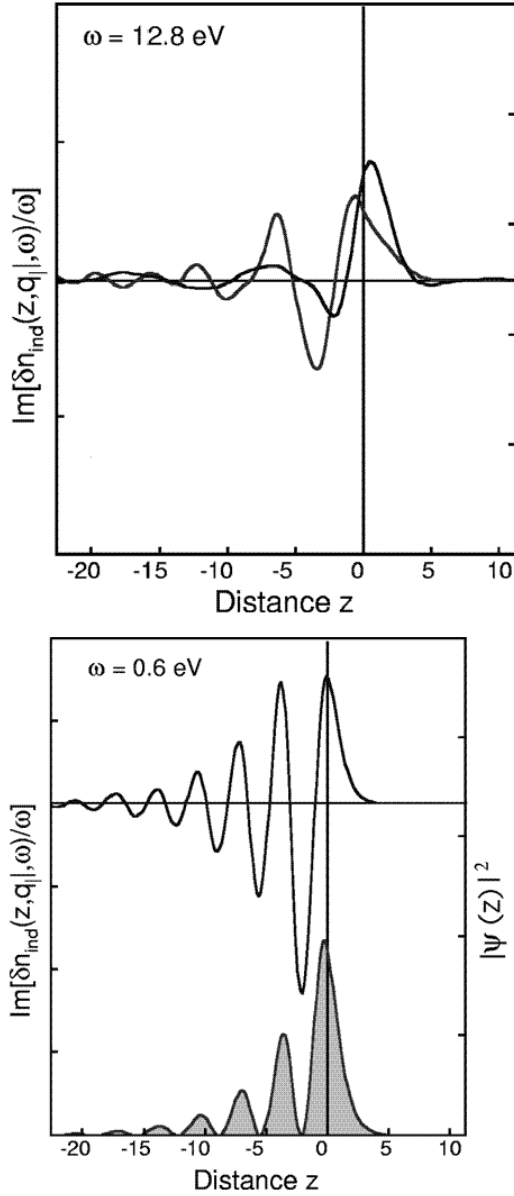


Figure 11. The RPA calculation of the imaginary part of the electron density induced in the (0001) surface of Be (black lines), as obtained from equations (37) and (38) for a wavevector of magnitude $q = 0.05 a_0^{-1}$, as a function of the z coordinate normal to the surface. The frequency has been chosen to be $\omega = 0.6$ eV (bottom panel) and $\omega = 12.8$ eV (top panel). The grey line in the top panel represents the corresponding jellium density-functional calculation for a semi-infinite free-electron gas. The probability density of the partially occupied Shockley surface state is represented in the bottom panel by a shaded area. As in figure 10, the crystal edge ($z = 0$) is chosen to be located half a lattice spacing beyond the last atomic layer, and $z < 0$ corresponds to the interior of the solid.

3D system yields a *new* distinct mode whose energy lies just above the upper edge $\omega_u^{2D} = v_F^{2D} q + q^2/2$ of the continuum of 2D e-h pair excitations (shaded area), where momentum and energy conservation allows e-h pairs to be created within the 2D electron gas.

For a well-defined acoustic surface plasmon to occur, it must exist for wavevectors \mathbf{q} and energies ω where decay cannot occur by exciting e-h pairs in the medium. Electron-

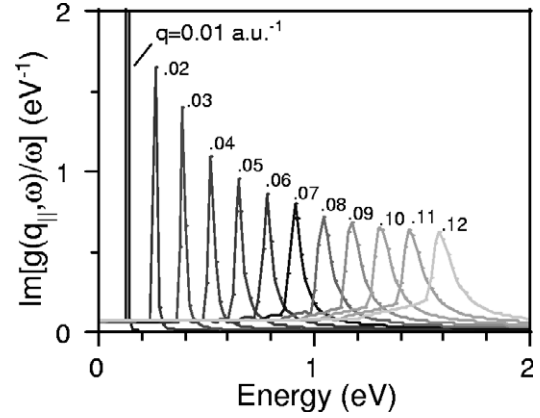


Figure 12. The energy-loss function $\text{Im}[g(q, \omega)]/\omega$ of Be(0001) versus the energy ω , as obtained from equation (39) for various values of the wavenumber q , in units of the inverse Bohr radius a_0^{-1} . The peaks are dictated by the corresponding poles of the surface-response function $g(q, \omega)$. In the long-wavelength ($q \rightarrow 0$) limit, $g(q, \omega)$ is simply the total electron density induced by the potential of equation (38).

hole pairs can be excited either within the 2D surface-state band, or within the 3D continuum of bulk states, or by promoting an electron from an occupied bulk state to an unoccupied 2D surface state. These three mechanisms for the production of e-h pairs at low energies are illustrated in figure 13.

- (i) Since the energy of acoustic surface plasmons always lies just above the upper edge ω_u^{2D} of the 2D e-h pair continuum (the shaded area in the bottom panel of figure 13), they cannot possibly decay by creating e-h pairs within the 2D band.
- (ii) The 3D Fermi velocity v_F^{3D} is typically larger than the Fermi velocity v_F^{2D} of the 2D surface-state band. This means that acoustic surface plasmons can decay by exciting e-h pairs within the 3D continuum of bulk states. However, at the low energies involved the probability for this process to occur is small [43].
- (iii) An inspection of the upper panel of figure 13 shows that, due to the presence of the band gap, for optical ($q = 0$) transitions to occur from an occupied 3D bulk state to an unoccupied 2D surface state a minimum energy is required, which decreases as the momentum transfer q increases. The region of momentum space where transitions from 3D to 2D states cannot occur corresponds to the area below the thin solid curve in the bottom panel of figure 13.

Figure 13 shows that at long wavelengths with $q < 0.06 a_0^{-1}$ acoustic surface plasmons can neither decay by exciting 2D e-h pairs nor decay by exciting 3D-2D e-h pairs, which results in a very well-defined collective excitation (see figure 12). At shorter wavelengths ($q > 0.06 a_0^{-1}$), the promotion of electrons from occupied 3D bulk states to unoccupied 2D surface states becomes possible and the corresponding plasmon peak broadens considerably.

6.3. Excitation of acoustic surface plasmons

We close this paper by discussing whether acoustic surface plasmons can be observed. As in the case of conventional

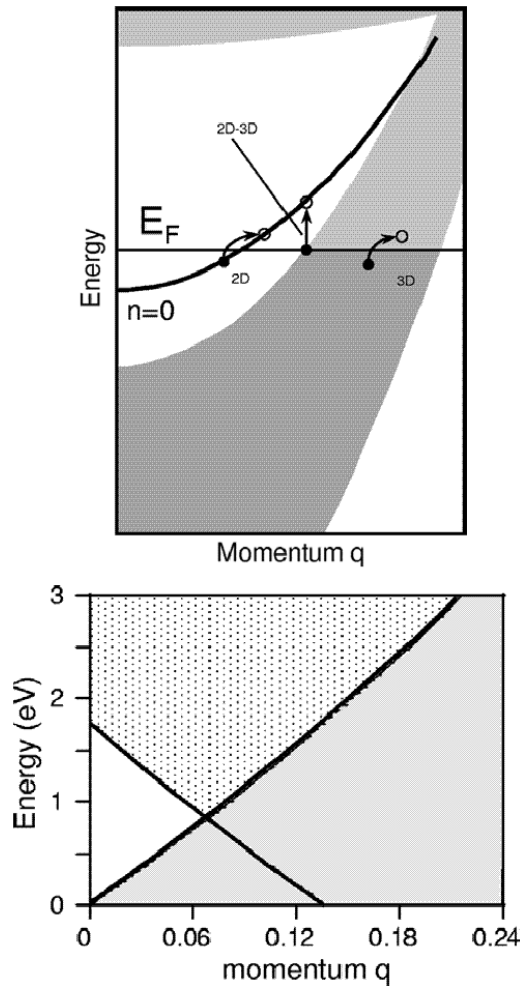


Figure 13. Top panel: a schematic representation of the projection of the bulk bands onto a solid surface that supports a partially occupied Shockley surface-state band. The energy of occupied and unoccupied states is displayed as a function of the momentum parallel to the surface. The solid curve represents a Shockley surface state. Dark and light shaded areas represent occupied and unoccupied bulk states, respectively. The white area represents the band gap. Electron–hole pair excitations are represented by arrows, depending on whether they correspond to transitions within the surface-state band (2D), transitions within the bulk bands (3D), or transitions from bulk to surface states (2D–3D). Bottom panel: the dispersion of the acoustic surface collective excitation of Be(0001), as derived from the peaks that are visible in figure 12 (thick solid curve). This curve stays just over the upper edge $\omega_u^{2D} = v_F^{2D} q + q^2/2$ of the 2D e–h pair continuum (shaded area). Momentum and energy conservation prevent 2D e–h pairs from being produced for energies above ω_u^{2D} . The area below the thin solid line represents the region of momentum space where transitions from 3D to 2D states cannot occur. Well-defined acoustic plasmons are expected to occur at wavevectors with magnitude smaller than $q \sim 0.06 a_0^{-1}$.

surface plasmons, acoustic surface plasmons should be expected to be excited by either electrons or light. Here we focus on a possible mechanism that would lead to the excitation of acoustic surface plasmons by light in, e.g., vicinal surfaces with high indices.

The top panel of figure 14 exhibits the energy dispersion of acoustic surface plasmons at low wavevectors. Also shown in this figure are the light line $\omega = cq$ and, for comparison,

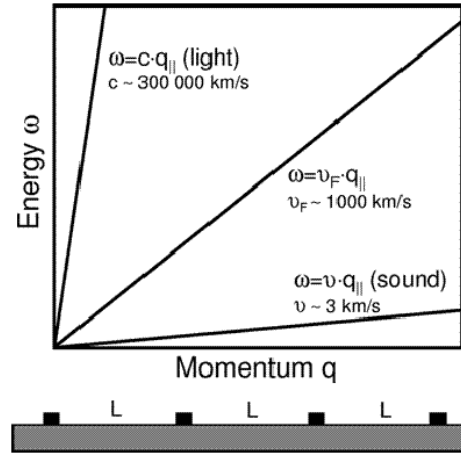


Figure 14. Top panel: a schematic (out of scale) representation of typical energy dispersions of acoustic surface plasmons, acoustic phonons, and free-space electromagnetic radiation. In the actual scale, the dispersion lines of free light and acoustic phonons should be very close to the vertical and horizontal axes, respectively. Bottom panel: a periodic grating of constant L . The grating periodic structure can provide the impinging free electromagnetic radiation with additional momentum $2\pi/L$.

a typical energy dispersion of acoustic phonons. The sound velocity of acoustic surface plasmons, which is close to the Fermi velocity of the 2D surface-state band, is typically a few orders of magnitude larger than the sound velocity of acoustic phonons in metals but still about two orders of magnitude smaller than the velocity of light.

The acoustic surface-plasmon dispersion curve is well below the dispersion curve of free-space electromagnetic radiation. Hence, there is, in principle, no way that incident light can provide an ideal surface with the correct amount of momentum and energy for the excitation of an acoustic surface plasmon. As in the case of conventional surface plasmons, however, a periodic corrugation or grating in the metal surface should be able to provide the missing momentum.

If light hits a surface with a periodic corrugation, the grating (see bottom panel of figure 14) can provide the impinging free electromagnetic waves with additional momentum arising from the grating periodic structure. If free electromagnetic radiation hits the grating at an angle θ , its wavevector along the grating surface has magnitude

$$q = \frac{\omega}{c} \sin \theta \pm \frac{2\pi}{L} n, \quad (40)$$

where L represents the grating constant, and $n = 1, 2, \dots$. Hence, the linear (nearly vertical) dispersion relation of free light changes into a set of parallel straight lines, which can match the acoustic plasmon dispersion relation.

For a well-defined acoustic surface plasmon in Be(0001) to be observed, the wavenumber q needs to be smaller than $q \sim 0.06 a_0^{-1}$. For $q = 0.05 a_0^{-1}$, equation (40) with $n = 1$ yields a grating constant $L = 66 \text{ \AA}$. Acoustic surface plasmons of energy $\omega \sim 0.6 \text{ eV}$ could be excited in this way. Although a grating period of a few nanometres sounds unrealistic with present technology, the possible control of vicinal surfaces with high indices could provide appropriate grating periods in the near future. Alternatively, acoustic surface plasmons could be

observed with the use of high-resolution electron energy-loss spectroscopy (EELS) under grazing incidence.

Acknowledgments

Partial support by the University of the Basque Country, the Basque Unibertsitate eta Ikerketa Saila, the Spanish Ministerio de Educación y Cultura, and the Max Planck Research Award Funds is gratefully acknowledged.

References

- [1] Pines D and Bohm D 1952 *Phys. Rev.* **85** 338
- [2] Pines D 1956 *Rev. Mod. Phys.* **28** 184
- [3] Gabor D 1956 *Phil. Mag.* **1** 1
- [4] Ritchie R H 1957 *Phys. Rev.* **106** 874
- [5] Stern E A and Ferrell R A 1960 *Phys. Rev.* **120** 130
- [6] Powell C J and Swan J B 1959 *Phys. Rev.* **115** 869
Powell C J and Swan J B 1959 *Phys. Rev.* **116** 81
- [7] Feibelman P J 1971 *Surf. Sci.* **27** 438
- [8] Ritchie R H 1972 *Phys. Lett. A* **38** 189
- [9] Ray R and Mahan G D 1972 *Phys. Lett. A* **42** 306
- [10] Sunjic A, Toulouse G and Lucas A A 1972 *Solid State Commun.* **11** 1629
- [11] Schmit J and Lucas A A 1972 *Solid State Commun.* **11** 415
- [12] Echenique P M and Pendry J B 1975 *J. Phys. C: Solid State Phys.* **8** 2936
- [13] Echenique P M, Ritchie R H, Barberan N and Inkson J 1981 *Phys. Rev. B* **23** 6486
- [14] Feibelman P J 1982 *Prog. Surf. Sci.* **12** 287
- [15] Ritchie R H 1963 *Prog. Theor. Phys.* **29** 607
- [16] Ritchie R H and Marusak A L 1966 *Surf. Sci.* **4** 234
- [17] Beck D E 1971 *Phys. Rev. B* **4** 1555
- [18] Hohenber P and Kohn W 1964 *Phys. Rev.* **136** B864
Kohn W and Sham L J 1965 *Phys. Rev.* **140** A1133
- [19] Tsuei K-D, Plummer E W, Liebsch A, Kempa K and Bakshi P 1989 *Phys. Rev. Lett.* **64** 44
- [20] Plummer W, Tsuei K-D and Kim B-O 1995 *Nucl. Instrum. Methods B* **96** 448
- [21] Benett A J 1970 *Phys. Rev. B* **1** 203
- [22] Ritchie R H and Eldridge H B 1962 *Phys. Rev.* **126** 1935
- [23] Teng Y-Y and Stern E A 1967 *Phys. Rev. Lett.* **19** 511
- [24] Otto A 1968 *Z. Phys.* **216** 398
- [25] Kretschmann E and Raether H 1968 *Z. Naturf. a* **23** 2135
- [26] Sambles J R, Bradbery G W and Yang F Z 1991 *Contemp. Phys.* **32** 173
- [27] Berndt R, Gimzewski J K and Johansson P 1991 *Phys. Rev.* **67** 3796
- [28] Shea M J and Compton R N 1993 *Phys. Rev. B* **47** 9967
- [29] Rocca M 1995 *Surf. Sci. Rep.* **22** 1
- [30] Rothenhausler B and Knoll W 1988 *Nature* **332** 615
- [31] Schuster S C, Swanson R V, Alex L A, Bourret R B and Simon M I 1993 *Nature* **365** 343
- [32] Pendry J B 1999 *Science* **265** 1687
- [33] Ebbesen T W, Lezec H J, Ghaemi H F, Thio T and Wolff P A 1998 *Nature* **391** 667
- [34] Lezec H J, Degiron A, Devaux E, Linke R A, Martin-Moreno L, García-Vidal F J and Ebbesen T W 2002 *Science* **297** 820
- [35] Barnes W L, Dereux A and Ebbesen T W 2003 *Nature* **424** 824
- [36] Pines D 1956 *Can. J. Phys.* **34** 1379
- [37] March N H and Tosi M P 1995 *Adv. Phys.* **44** 299
- [38] Das Sarma S and Madhukar A 1981 *Phys. Rev. B* **23** 805
- [39] Olego D, Pinczuk A, Gossard A C and Wiegmann W 1985 *Phys. Rev. B* **32** 1921
- [40] Ruvalds J 1987 *Phys. Rev. B* **35** 8869
Ruvalds J 1987 *Nature* **328** 299
- [41] Bill A, Morawitz H and Kresin V Z 2002 *Phys. Rev. B* **66** 100501
- [42] Silkin V M, García-Lekue A, Pitarke J M, Chulkov E V, Zaremba E and Echenique P M 2004 *Europhys. Lett.* **66** 260
- [43] Pitarke J M, Nazarov V U, Silkin V M, Chulkov E V, Zaremba E and Echenique P M 2004 *Phys. Rev. B*, at press
- [44] Flores F and García Moliner F 1979 *Introduction to the Theory of Solid Surfaces* (Cambridge: Cambridge University Press)
- [45] Fetter A L and Wallecka J D 1964 *Quantum Theory of Many-Particle Systems* (New York: McGraw-Hill)
- [46] Lindhard J and Dan K 1954 *Vidensk. Selsk. Mat. Fys. Medd.* **28** 8
- [47] See, e.g. Liebsch A 1997 *Electronic Excitations at Metal Surfaces* (New York: Plenum)
- [48] Ferrell R A 1958 *Phys. Rev.* **111** 1214
- [49] Stern F 1967 *Phys. Rev. Lett.* **18** 546
Ando T, Fowler A B and Stern F 1982 *Rev. Mod. Phys.* **54** 437
- [50] Allen S J Jr, Tsui D C and Logan R A 1977 *Phys. Rev. Lett.* **38** 980
- [51] Nagao T, Heldebrandt T, Henzler M and Hasegawa S 2001 *Phys. Rev. Lett.* **86** 5747
- [52] Abramowitz M and Stegun I A 1965 *Handbook of Mathematical Functions* (New York: Dover)
- [53] Nuñez R, Echenique P M and Ritchie R H 1980 *J. Phys. C: Solid State Phys.* **13** 4229
- [54] Ibach H and Mills D L 1982 *Electron Energy Loss Spectroscopy and Surface Vibrations* (New York: Academic)
- [55] Tsuei K-D, Plummer E W, Liebsch A, Pehlke E, Kempa K and Bakshi P 1991 *Surf. Sci.* **247** 302
- [56] Sprunger P T, Watson G M and Plummer E W 1992 *Surf. Sci.* **269** 551
- [57] Zaremba E and Kohn W 1976 *Phys. Rev. B* **13** 2270
- [58] Apell P and Holmberg C 1984 *Solid State Commun.* **49** 693
- [59] Tarriba J and Mochan W L 1992 *Phys. Rev.* **46** 12902
- [60] Feibelman P J 1993 *Surf. Sci.* **282** 129
- [61] Liebsch A 1993 *Phys. Rev. Lett.* **71** 145
- [62] Apell S P, Echenique P M and Ritchie R H 1995 *Ultramicroscopy* **65** 53
- [63] Ronveaux A, Moussiaux A and Lucas A A 1977 *Can. J. Phys.* **55** 1407
- [64] Kroto H W, Heath J R, O'Brien S C, Curl R F and Smalley R E 1985 *Nature* **318** 162
- [65] Ijima S 1991 *Nature* **354** 56
- [66] Östling D, Apell P and Rosén A 1993 *Europhys. Lett.* **21** 539
- [67] Raether H 1988 *Surface Plasmons (Springer Tracts in Modern Physics vol 111)* (Berlin: Springer)
- [68] Inglesfield J E 1982 *Rep. Prog. Phys.* **45** 223
- [69] Chaplik A V 1972 *Zh. Eksp. Teor. Fiz.* **62** 746
Chaplik A V 1972 *Sov. Phys.—JETP* **35** 395 (Engl. Transl.)
- [70] Chulkov E V, Silkin V M and Echenique P M 1999 *Surf. Sci.* **437** 330
- [71] Echenique P M, Pitarke J M, Chulkov E V and Rubio A 2000 *Chem. Phys.* **251** 1